ISSN 1063-780X, Plasma Physics Reports, 2017, Vol. 43, No. 3, pp. 324–329. © Pleiades Publishing, Ltd., 2017.
Original Russian Text © Yu.V. Martynenko, 2017, published in Fizika Plazmy, 2017, Vol. 43, No. 3, pp. 260–266.

PLASMA–SURFACE INTERACTION

Metal Droplet Erosion and Shielding Plasma Layer under Plasma Flows Typical of Transient Processes in Tokamaks

Yu. V. Martynenko*

National Research Nuclear University "MEPhI," Moscow, 115409 Russia
National Research Center Kurchatov Institute, Moscow, 123182 Russia
**e-mail: Martynenko_YV@nrcki.ru*

Received March 16, 2016

Abstract—It is shown that the shielding plasma layer and metal droplet erosion in tokamaks are closely interrelated, because shielding plasma forms from the evaporated metal droplets, while droplet erosion is caused by the shielding plasma flow over the melted metal surface. Analysis of experimental data and theoretical models of these processes is presented.

DOI: 10.1134/S1063780X17030084

1. INTRODUCTION

Erosion of the first wall and divertor is a key problem for creating the ITER tokamak reactor. These tokamak elements are subject to the most intense plasma–heat action during fast transient phenomena, such as ELM (edge localized mode) events and current disruptions. Heat loads on the ITER divertor plates are expected to be $Q = 0.2–5$ MJ/m^2 for 0.1–1 ms during ELM events and $Q = 10–100$ MJ/m^2 for 1–10 ms during current disruptions [1, 2]. Such heat loads are close to those in quasi-steady plasma accelerators (QSPAs) [3].

However, the pressure of QSPA plasma flows differs substantially from that in ITER ELMs and disruptions. The pressure of plasma flows is expected to be $10^2–10^3$ Pa during ITER ELMs and $10^2–4 \times 10^3$ Pa during ITER disruptions, whereas the pressure of QSPA plasma flows reaches several units of 10^5 Pa (several atmospheres). Below, it will be shown when such a difference in the pressures is of importance.

The most dangerous kinds of erosion are cracking and brittle failure of metal surfaces [4], as well as transfer of the melted metal from one place to another [5, 6]. The latter mechanism is responsible for the strongest thinning of the facing material of the first wall and divertor and exceeds droplet erosion by one order of magnitude [5, 6]. Transfer of the melted layer also leads to the welding of the neighboring constructional elements. At the same time, at temperatures below the boiling temperature, droplet erosion is the main mechanism for the mass loss of the divertor and wall material, exceeding its sputtering and evaporation.

2. ANALYSIS OF THE EXPERIMENTAL DATA ON METAL EROSION

In recent years, considerable attention has been paid to the shielding of targets by the evaporated metal plasma. It was shown in [7, 8] that, as the intensity of the primary plasma flow increases, the energy absorbed by the target reaches saturation. The absorbed energy densities for tungsten and graphite in the saturation regime turned out to be nearly the same, $Q_{abs} = 0.4–0.5$ MJ/m^2 (Fig. 1). At the same time, at power flux densities of the primary flow corresponding to saturation, the fast loss of the target mass occurs [9] (Fig. 2).

We note that, even if all erosion products were atoms (in fact, the main erosion products are droplets, which carry away a substantially lower energy), the energy carried away by the erosion products is much lower than the absorbed energy. Therefore, it is incorrect to consider that saturation of energy absorption is caused by evaporative cooling of the target.

Evaporation from the surface plays an insignificant role, because the motion of the melted layer does not allow the temperature to increase much higher than the melting temperature. For tungsten and beryllium, evaporation at such a temperature is much lower than it is required to explain the observed mass loss. The data from [5] on the transfer of the upper hot layer of melted metal from the center of the irradiated region toward the periphery indicate that the surface temperature exceeds the melting temperature T_m by only 200°–300°. The removal of a surface layer of thickness h over a time τ means that the density of the heat flux

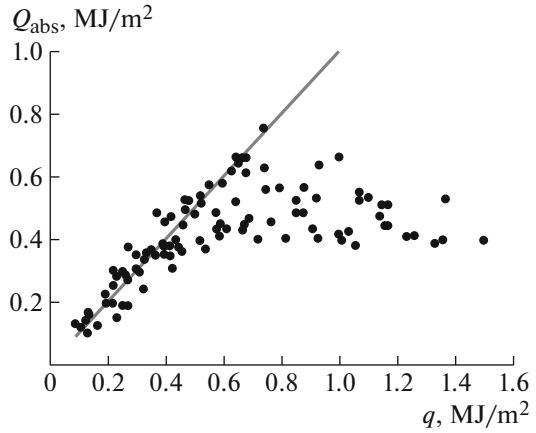

Fig. 1. Energy absorbed by a tungsten target irradiated by a pulsed plasma flow with a duration of 50 μs in the MK-200 plasma accelerator as a function of the energy density of the plasma flow.

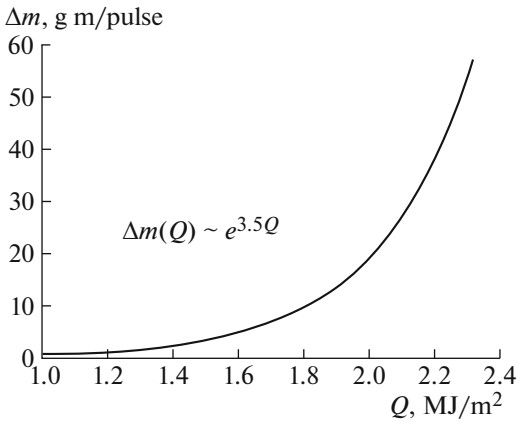

Fig. 2. Specific mass loss Δm of a tungsten target irradiated by a pulsed plasma flow with a duration of 0.5 ms in QSPA as a function of the energy density of the plasma flow.

carried away from the surface is $Q_- = (h/\tau)\rho C\Delta T$, where ΔT is the temperature drop in the surface layer of thickness h, ρ is the mass density of the metal, and C is the heat capacity. It can be assumed that the surface temperature exceeds the melting temperature T_m by ΔT. As the primary plasma power flux Q onto the surface shielded by the plasma grows, the absorbed power flux Q_{abs} saturates at $Q_{abs} = 0.5$ MJ/m^2. Equating Q_- and Q_{abs}, we find that the surface temperature is $T = T_m + Q_{abs}\tau/\rho hC$. For most metals, the temperature drop under conditions of QSPA pulses amounts to $Q_{abs}\tau/\rho hC = 200°–300°$. Calculations show that, for tungsten and beryllium, the mass loss due to evaporation from the surface is two orders of magnitude lower than that measured after target irradiation by plasma in QSPA experiments [5, 6] (see table).

A wavy relief observed after target irradiation by plasma flows and droplets flying away from the target allow us to assume that droplet erosion is the origin of the mass loss. An obvious evidence of droplet emission is given in [5]. Figure 3 shows the distribution of droplets over size under irradiation of tungsten in by QSPA plasma. However, the total volume of all droplets in [5] did not provide the observed mass loss. At $Q =$ 1.6 MJ/m^2, the tungsten mass loss measured in [5] was $\Delta m \approx 5$ g/m^2 per pulse. In this case, about 100 droplets with an average size of 30 μm were emitted from the irradiated area of radius 3 cm, which corresponded to a mass loss of $\Delta m \approx 2 \times 10^{-2}$ g/m^2 per pulse.

In the early experiments [10], carried out at the MKT plasma accelerator with a shorter plasma pulse of 60 μs but a rather large energy flux of 300 kJ/m^2, emission of tungsten droplets with a size of ~1 μm and less (Fig. 4) was observed. The number of droplets per cm^2 was 10^7–10^9. It is impossible to directly compare mass losses in the experiments carried out at QSPA and MKT because of the difference in the plasma pulse parameters; however, estimates show that the mass carried away by small droplets is substantially larger than that carried away by large (~30 μm) droplets, which can explain the observed mass loss.

In [6], two hydrodynamic mechanisms of droplet erosion at temperatures in the melted metal layer below the boiling temperature were noted. Both mechanisms are consequences of plasma motion over the melted metal layer, which leads to the formation of waves due to Kelvin–Helmholtz (KH) instability. The first mechanism [11] is associated with the blowing-off of the wave crests by the plasma wind. It was assumed in [11] that this mechanism was responsible for the emission of droplets with sizes of ~1 μm. The second mechanism is a consequence of wave motion under the action of the plasma flow pressure. Due to inhomogeneities arising in the waves, they propagate with different velocities and come up on one another; as a result, droplets with sizes on the order of the wavelength (i.e., exactly such as those observed in [5]) are ejected from the surface. Droplets can also be emitted when the melted layer is heated to the boiling tempera-

Table

	N_{dr}, m^{-2}	Δm, g/m^2	Δm_{vapor}, g/m^2	Δm, g/m^2 (experiment)	r_{max}, μm
W, $P_0 = 3$ atm	5×10^{12}	20	6×10^{-2}	3–9	30
Be, $P_0 = 2$ atm	4×10^{14}	10	$(4.5–7) \times 10^{-3}$	0.1–0.35 $P \approx 1$ atm	37

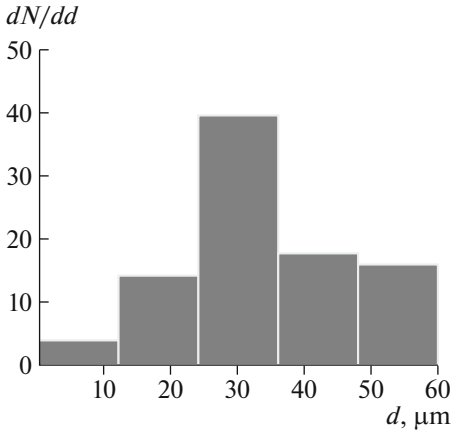

Fig. 3. Distribution of tungsten droplets over sizes. Target irradiation by a pulsed plasma flow with an energy density of 1.6 MJ/m^2 and a duration of 0.2–0.6 ms in QSPA.

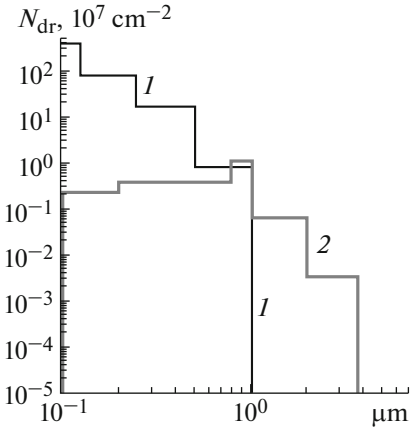

Fig. 4. Distribution of tungsten droplets over sizes: (*1*) droplets flying parallel to the surface and collected by a Si collector and (*2*) droplets flying nearly along the normal to the surface and collected by a basalt filter. Target irradiation by 10 deuterium plasma pulses with an energy density of 300 kJ/m^2 and a duration of 60 μs in MKT.

ture, which however takes place only for low-melt metals. For most metals, droplets are emitted already at a temperature only slightly exceeding the melting temperature.

3. WAVES ON THE MELTED METAL SURFACE

As was said above, the considered mechanisms of droplet emission are associated with the generation of waves in the melted metal layer due to the development of KH instability (see [12]) when the primary plasma propagates away from the center of the flow toward the periphery above the melted layer. The length of excited waves λ, their frequency ω, and growth rate γ are

$$\lambda = \frac{3\pi\alpha}{2P}, \quad (1)$$

$$\omega = \frac{2^{5/2}}{3}\frac{P^{3/2}}{\alpha\rho^{1/2}}\left(\frac{\rho'}{\rho}\right)^{1/2}, \quad (2)$$

$$\gamma = \frac{2^{5/2}}{3^{3/2}}\frac{P^{3/2}}{\alpha\rho^{1/2}}, \quad (3)$$

where α is the surface tension of the melted metal; $P = \rho' U^2/2$ is the plasma flow pressure; ρ' and U are the plasma density and velocity, respectively; and ρ is the mass density of the metal. We note that, for the pulse plasma duration τ, the wave structure can form ($\gamma > 1/\tau$) only if the plasma flow pressure exceeds the critical value,

$$P > P_{cr} = 0.94\alpha^{2/3}\rho^{1/3}\tau^{-2/3}. \quad (4)$$

It follows from conditions (4) that, for KH instability to develop over a time of $\tau \approx 1$ ms on the melted tungsten surface, the plasma flow pressure over the melted surface should be $P > 7 \times 10^3$ Pa. In this case, the maximum wavelength is $\lambda_{max} = 0.15$ mm. For beryllium, we have $P > 2.2 \times 10^3$ Pa and $\lambda_{max} = 3$ mm. The frequency ω is lower than the growth rate γ by a factor of $(3\rho/\rho')^{1/2} \approx 10^3$, i.e., the oscillatory wave process is not implemented.

When the primary plasma flow with a pressure P_0 is incident along the normal onto the target surface, the pressure force acting on the target also has the normal component. In this case, the energy of $P_0 H\lambda$ is required to generate waves with a height H and wavelength λ, which hampers the development of instability. Following the derivation of the condition for the onset of KH instability given in [12], it is easy to show that, in this case, in formulas (1)–(3), the plasma flow pressure P parallel to the surface should be replaced with $P_{eff} = P - P_0/2$. In the center of the target, we have $P_{eff} < 0$, i.e., the development of instability is impossible, which was indeed observed in the surface relief formed under target irradiation (see Fig. 5).

4. EMISSION OF DROPLETS

Let us now consider emission of droplets due to the blowing-off of the wave crests. The plasma flow moves over the melted metal waves with a velocity much higher than the wave velocity and blows off the wave crests in the form of droplets. When the pressure force of the plasma wind P acts on the wave over a time t, the wave crest with the height

$$\Delta = (\nu t)^{1/2}, \quad (5)$$

where ν is the kinematic viscosity, behaves as a liquid on a solid base. If the wave crest shifts during the time t over the distance equal to its base d, then it is detached from the wave and blown off in the form of a droplet. Assuming that the plasma pressure force is

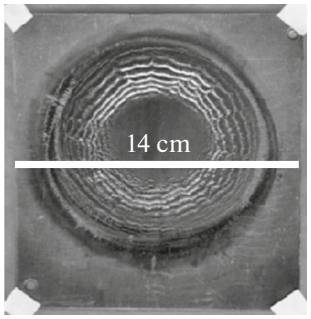

Fig. 5. Surface of a niobium target after irradiation in QSPA by a series of plasma pulses incident along the normal to the target with the energy density Q progressively increasing from 0.5 to 4.5 MJ/m^2.

equal to the surface tension [6], we find the length of the base of the wave crest is

$$d = (r_1\Delta)^{1/2}, \quad (6)$$

where $r_1 = \alpha/P$ is the curvature radius of the crest. The time during which the crest shifts over the distance d is

$$t = \left(\frac{2d}{a}\right)^{1/2}, \quad (7)$$

where $a = P/\rho d$ is the acceleration of the wave crest. Equating the times t in expressions (5) and (7), we find the height of the detached crest,

$$\Delta = (2\alpha\rho\nu^2)^{1/3}P^{-2/3}. \quad (8)$$

We note that the wave crest reaches the velocity $v = P\Delta^2/\rho\nu d$, at which the force of the plasma wind pressure is counterbalanced by the friction force, exactly at the time at which the crest is detached from the wave, i.e., the detachment occurs in the acceleration mode.

The wave crests are detached one after another with time intervals t. The wave height is limited by the blowing-off of the wave crest. Equating the rise rate of the wave height $H\gamma$ and the rate of its decrease due to the blowing-off of the wave crests, Δ/t, we find the maximum height of the wave,

$$H_m = \frac{\Delta}{\gamma t} = 0.8(\nu\alpha^2\rho^{1/2})^{1/3}P^{-5/6}. \quad (9)$$

The wave crest is blown off from the entire wave front, after which the detached wave crest splits into droplets with a volume of $\sim(\Delta d)^{3/2}$. Therefore, the detachment of the crest of one concentric wave of radius R leads to the emission of $\pi R/(\Delta d)^{1/2}$ droplets with a size

$$r = (\Delta d)^{1/2} = (2\rho)^{1/4}(\alpha\nu)^{1/2}P^{-3/4}. \quad (10)$$

The droplet size is limited from below by the size of droplets emitted at the maximum plasma flow pressure, $r_{\min} \approx r(P_0)$. The maximum droplet size $r_{\max}$ is observed at the periphery, where the plasma flow pressure is equal to the critical pressure P_{cr}, below which waves are not generated. It is seen from the table that the blowing-off of the wave crests can result in the emission of fairly large droplets.

The number of droplets emitted per pulse per unit area of the melted metal surface is

$$N_{dr}(P) = \frac{\tau}{t\lambda r} = \tau\frac{2^{1/12}}{3\pi}\nu^{-5/6}\alpha^{-13/6}\rho^{-11/12}P^{37/12}. \quad (11)$$

Assuming that the radial profile of the plasma flow pressure is $P \sim P_0\exp(-R^2/\sigma^2)$, we find the distribution of droplets over size,

$$\frac{dN_{dr}}{dr} = \frac{dN_{dr}}{dR}2pR\frac{dR}{dr} \approx \tau\nu^{23/18}\alpha^{-1/9}\rho^{1/9}P_0^{37/24}\sigma^2 r^{-46/9}. \quad (12)$$

Distribution (12) is a steeper descending function than the distribution $dN_{dr}/dr \sim r^{-2.5}$, observed in the MKT experiments [12]. However, small droplets evaporate faster and return back onto the target under the action of the plasma pressure, due to which the actual distribution is depleted with small droplets.

The mass loss per pulse due to droplet erosion is

$$\Delta m = \rho\tau\int r^3\left(dN_{dr}/dr\right)dr \sim P_0^{25/8}. \quad (13)$$

Thus, the mass loss grows rapidly with increasing plasma flow pressure over the melted surface. In the experiments [5], a strong dependence of the mass loss on the power flux density of the primary plasma flow, $\Delta m \sim \exp(3.5Q)$, was observed. However, as will be shown below, the plasma flow pressure over the melted surface depends nonlinearly on the power flux density of the primary plasma flow. The table presents the number of droplets N_{dr} emitted per QSPA pulse with a duration of $\tau = 0.5$ ms at the pressure of the primary plasma flow corresponding to the power flux density twice as high as the melting threshold. The table also gives the mass loss calculated by formula (13), the mass loss due to evaporation from the surface, and the mass loss measured experimentally [5], as well as the maximum size of droplets formed due to the blowing-off of the wave crests.

The calculated mass loss exceeds substantially the measured value, which can be explained by the return of droplets back onto the target, as well as by the condensation of supersaturated vapor over the melted surface.

5. NEAR-SURFACE LAYER OF THE SHIELDING PLASMA

Excitation of instability and generation of waves on the melted metal surface are obviously determined by the near-surface layer of the shielding plasma with a thickness only slightly exceeding the wavelength, $L > \lambda$. As will be shown below, the temperature and

density of this layer are $T \approx 1$ eV and $n = 10^{24}$–10^{25} m^{-3}, respectively. At the same time, the measured [8] density of the shielding plasma at a distance of ~1 cm from the target was $n = 2 \times 10^{23}$ m^{-3} and decreased rapidly with distance from the surface; i.e., the shielding plasma layer exciting KH instability is thinner than 1 cm. Therefore, we assume that the thickness of this layer is $L \sim 1$ mm.

Saturation of the power absorbed by the target means that the near-surface plasma layer is optically dense. Then, the temperature of the near-surface plasma layer can be found from the absorbed power flux density as

$$T = \left(\frac{W_{abs}}{\sigma_{SB}}\right)^{1/4}, \quad (14)$$

where σ_{SB} is the Stefan–Boltzmann constant, $W_{abs} = Q_{abs}/\tau$ is the absorbed power in the saturation regime. For $W_{abs} \approx 1$ GW/m^2 [8], we have $T \approx 1$ eV. We note that energy transfer from the shielding plasma layer to the surface by particles is weaker than radiative transfer. Assuming that W_{abs} is constant (although W_{abs} was measured only for tungsten and carbon), we will consider that the temperature of the near-surface plasma layer is also constant, $T \approx 1$ eV.

Since the main mechanism of the mass loss from the melted surface is emission of droplets, it can be expected that the near-surface layer forms from the evaporated droplets. Estimates show that detached tungsten droplets with sizes of $r < 1$ μm and velocities of about $H\gamma$ are evaporated in a 1-mm-thick layer. As droplets with sizes larger than 1 μm fly trough the near-surface plasma layer, they decrease in size by ~1 μm.

At a fixed temperature of the near-surface plasma layer, the pressure in it is determined by its density. The density of the near-surface plasma layer n can be found from the condition of the continuity of the flow. For the shielding plasma expanding along the normal to the surface, we have

$$n = \frac{q}{v_{exp}}, \quad (15)$$

where $q = \Delta m/M\tau$ is the flux of evaporated droplets, M is the mass of the meal atom, and v_{exp} is the expansion velocity. Since the main mass loss is determined by evaporation of small droplets, Δm can be taken equal to the total mass loss for estimates. The plasma expansion velocity is

$$v_{exp} = \left[v_T^2 - \frac{P_{ext}}{\rho'}\right]^{1/2}, \quad (16)$$

where v_T is the thermal velocity and P_{ext} is the external pressure. Then, the pressure in the near-surface plasma layer is

$$P = \frac{P_{ext}}{2} + \left[\frac{P_{ext}^2}{4} + (Mqv_T)^2\right]^{1/2}. \quad (17)$$

It is seen from expression (17) that, at $q > P_{cr}/2Mv_T$, even in the absence of the external pressure ($P_{ext} = 0$), the pressure in the near-surface plasma layer is sufficient for the formation of a tangential flow resulting in the excitation of instability of the melted metal surface and droplet erosion.

Let us present several examples in which instability of the melted layer surface and its consequences were observed at pressures of the primary plasma flow lower than the critical pressure. First, droplet erosion under target irradiation in the MKT plasma accelerator (Fig. 4) occurred at a pressure of the primary plasma flow of $P_{ext} = 10^3$ Pa, while the critical pressure was $P_{cr} = 7 \times 10^3$ Pa. Second, a well-developed wave structure was observed in [4] on a steel surface irradiated in QSPA by radiation (rather than by the plasma flow), when $P_{ext} \approx 0$. Third, droplet emission after termination of the primary plasma flow, which lasted for $\tau = 0.5$ ms, was observed in [9]. The most intense droplet emission took place 1 ms after the beginning of the plasma pulse and lasted for 2 ms. This could be caused by the replenishment of the near-surface layer of the shielding plasma due to droplet erosion occurring in the absence of an external pressure and slowing down the cooling of the shielding plasma.

However, the development of the instability in the absence of an external pressure is not always possible. According to calculations, erosion of beryllium in this case is low and $q < P_{cr}/2Mv_T$. The experiments carried out using the QSPA-Be accelerator at the Bochvar High-Technology Scientific Research Institute of Inorganic Materials [13] showed that the wave structure and fast transfer of the melted layer were possible only under direct action of the QSPA plasma flow (Fig. 6a), while under the action of radiation with the same power, no wave structure formed (Fig. 6b). The rough surface in Fig. 6b is due to the exit on the target surface of crystallites formed under fast solidification of the melted surface layer [4].

It should be noted that, in the absence of an external pressure, instability can develop if the primary flow is incident along the normal to the target surface and the shielding plasma also expands along the normal. At grazing incidence of the primary plasma flow and in the presence of a magnetic field, the evaporated material in the near-surface shielding plasma layer expands in a different way. Each such case should be analyzed individually. For the expansion of the shielding plasma, the transverse dimensions of the irradiated region are of great importance. For too small irradiation region, the tangential expansion of the shielding

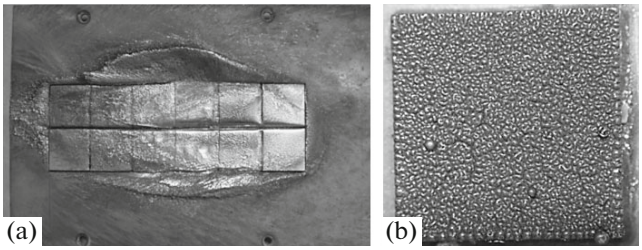

Fig. 6. Be sample after irradiation in the QSPA-Be plasma accelerator by (a) 40 and (b) 100 plasma pulses with Q = 0.5 MJ/m^2.

plasma does not allow the formation of the high pressure shielding plasma. The magnetic field with lines entering the target prevents expansion of the shielding plasma and favors the increase in its density and pressure. In this context, the question arises as to the optimal width of the plasma flow entering the divertor.

On the other hand, if the dense shielding plasma does not form, then no saturation of the energy absorbed by the target occurs. All these problems require thorough analysis.

6. CONCLUSIONS

The results of the present work can be summarized as follows.

1. If the pressure of the plasma flow parallel to the melted metal surface is higher than the critical pressure P_{cr} at which the growth rate of KH instability becomes larger than the inverse plasma pulse duration, $\gamma > \tau^{-1}$, then this flow (i) forms a wavy relief on the melted surface and (ii) blows off the wave crests, which leads to droplet erosion—the main mechanism for the mass loss of the target material.

2. Evaporation of droplets results in the formation of the secondary shielding plasma.

3. In the regime of saturation of the energy absorbed by the target, the temperature of the near-surface plasma layer is fixed at a level of $T \approx 1$ eV.

4. The density and pressure of the near-surface plasma layer are determined by the balance between the influx and expansion of the evaporated droplet material.

5. When the primary plasma flow is incident along the normal onto the target surface, even at pressures below P_{cr}, a dense near-surface plasma layer with a pressure higher than P_{cr} can form due to intense emission and evaporation of droplets.

6. At grazing incidence of the primary plasma flow and in the presence of a magnetic field, the expansion of the evaporated material of the near-surface layer of the shielding plasma requires a special study.

ACKNOWLEDGMENTS

The work was supported by the Program for Enhancement of Competitiveness of the National Research Nuclear University "MEPhI."

REFERENCES

1. ITER Physics Basis Editors, ITER Physics Expert Group Chairs and Co-Chairs, and ITER Joint Central Team and Physics Integration Unit, Nucl. Fusion **39**, 2137 (1999).
2. G. Federici, C. H. Scinner, and J. N. Brooks, Nucl. Fusion **41**, 1967 (2001).
3. H. Würz, N. I. Arkhipov, V. P. Bakhtin, I. Konkashbaev, I. Landman, V. M. Safronov, D. A. Toporkov, and A. M. Zhitlukhin, J. Nucl. Mater. **220–222**, 1066 (1995).
4. V. P. Budaev, Yu. V. Martynenko, L. N. Khimchenko, A. M. Zhitlukhin, N. S. Klimov, R. A. Pitts, I. Linke, N. E. Belova, A. V. Karpov, D. V. Kovalenko, V. L. Podkovyrov, and A. D. Yaroshevskaya, Plasma Phys. Rep. **39**, 910 (2013).
5. I. M. Poznyak, N. S. Klimov, V. L. Podkovyrov, V. M. Safronov, A. M. Zhitlukhin, and D. V. Kovalenko, Vopr. At. Nauki Tekh., Ser. Termoyad. Sintez, No. 4, 23 (1012).
6. Yu. V. Martynenko, Vopr. At. Nauki Tekh., Ser. Termoyad. Sintez, No. 2, 53 (2014).
7. V. M. Safronov, N. I. Arkhipov, I. S. Landman, S. E. Pestchanyi, D. A. Toporkov, and A. M. Zhitlukhin, J. Nucl. Mater. **386–388**, 744 (2009).
8. I. M. Poznyak, N. I. Arkhipov, S. V. Karelov, V. M. Safronov, and D. A. Toporkov, Vopr. At. Nauki Tekh., Ser. Termoyad. Sintez, No. 1, 70 (2014).
9. N. S. Klimov, V. L. Podkovyrov, A. M. Zhitlukhin, V. M. Safronov, D. V. Kovalenko, A. A. Moskacheva, and I. M. Poznyak, Vopr. At. Nauki Tekh., Ser. Termoyad. Sintez, No. 2, 52 (2009).
10. M. I. Guseva, V. M. Gureev, A. G. Domantovskii, Yu. V. Martyneno, P. G. Moskovkin, V. G. Stolyarova, V. M. Strunnikov, L. N. Plyashkevich, and V. I. Vasil'ev, Tech. Phys. **47**, 841 (2002).
11. Yu. V. Martynenko and P. G. Moskovkin, Vopr. At. Nauki Tekh., Ser. Termoyad. Sintez, No. 1, 65 (2000)
12. L. D. Landau and E. M. Lifshitz, *Fluid Mechanics* (Nauka, Moscow, 1986; Pergamon, Oxford, 1987).
13. V. M. Safronov, private communication.

Translated by L. Mosina